

Accepted Manuscript

Flexural moduli and end connection stiffnesses of symmetrically loaded GFRP beams for limit state serviceability design analysis

G.J. Turvey, Y-S. Zhang

PII: S0263-8223(17)34282-4

DOI: <https://doi.org/10.1016/j.compstruct.2018.05.081>

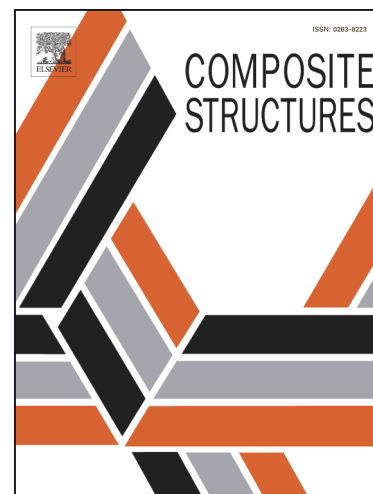
Reference: COST 9720

To appear in: *Composite Structures*

Received Date: 8 January 2018

Revised Date: 9 April 2018

Accepted Date: 17 May 2018



Please cite this article as: Turvey, G.J., Zhang, Y-S., Flexural moduli and end connection stiffnesses of symmetrically loaded GFRP beams for limit state serviceability design analysis, *Composite Structures* (2018), doi: <https://doi.org/10.1016/j.compstruct.2018.05.081>

This is a PDF file of an unedited manuscript that has been accepted for publication. As a service to our customers we are providing this early version of the manuscript. The manuscript will undergo copyediting, typesetting, and review of the resulting proof before it is published in its final form. Please note that during the production process errors may be discovered which could affect the content, and all legal disclaimers that apply to the journal pertain.

Flexural moduli and end connection stiffnesses of symmetrically loaded GFRP beams for limit state serviceability design analysis

G.J. Turvey*⁺ and Y-S. Zhang**

* Engineering Department, Lancaster University, Gillow Avenue, Lancaster LA1 4YW, UK

** Doosan Babcock, Porterfield Road, Renfrewshire, PA4 8DJ, UK

(⁺ Corresponding Author's Email Address: g.turvey@lancaster.ac.uk)

Abstract

An alternative analysis utilizing deflection, strain and curvature data from simply supported single-span three- and four-point bending tests is presented for determining the flexural modulus of a beam. The analysis is extended to beams with bolted end connections to determine their rotational stiffnesses. Analyses of tests on symmetrically loaded pultruded GFRP wide flange (WF) beams with bolted end connections formed from GFRP equal leg angles are shown to produce consistent and repeatable connection stiffnesses. The semi-rigid beam analysis is recast to quantify the reduction in serviceability limit loads with increasing beam slenderness. Deflection and load performance indices for symmetric four-point loading are derived and evaluated using the connection stiffness data. For each type of end connection, the reductions in mid-span deflection and increases in load, relative to simply supported end conditions, are quantified for a range of load spacing ratios.

Keywords: bolted end connections; elastic modulus; GFRP beams; joint stiffnesses; pultrusion; testing

1 Introduction

The use of pultruded glass fibre reinforced polymer (GFRP) composite beams in infrastructure applications is becoming more widespread as awareness of their advantageous characteristics (namely low self-weight, high corrosion resistance etc.) and confidence in the use of code-like design guidance [1 & 2] and pultruders' design manuals [3 – 5] increases amongst the structural engineering community.

Despite their many advantageous characteristics pultruded GFRP beams also suffer from a few disadvantageous characteristics, particularly low flexural stiffness compared to similar-sized metallic beams and lack of ductility. The consequence of these adverse characteristics is that the design of pultruded GFRP beams is stiffness rather than ultimate stress dominated. Hence, it is the maximum allowable/serviceability deflection or the local/lateral buckling load rather than the ultimate stress which tends to determine the maximum load that a pultruded GFRP beam is allowed to support and still satisfy its compliance requirements. Furthermore, as pultruded GFRP is an elastic-brittle material, it is the elastic flexural stiffness characteristics that are required for beam design. In particular, the longitudinal elastic modulus of the GFRP and the initial/linear rotational stiffness of the beam's end connections are the main stiffness characteristics required for their design. That said, it should also be appreciated that the shear modulus of GFRP is generally much lower than that of isotropic metals such as steel. Hence, deflections due to shear in pultruded GFRP beams may be significant, especially when the span to depth ratio is small (less than 10 – 20, depending on the axis of flexure) whereas in steel beams the effects of shear on deflections may generally be disregarded.

During the past three decades researchers have developed various experimental techniques for determining the elastic flexural and/or shear moduli of pultruded GFRP beam profiles. They generally involve flexure tests on simply supported beams. Details of three-point beam flexure tests, including instrumentation and loading procedures, for determining the elastic flexural and shear moduli are described in [6 & 7]. Symmetric four-point flexure tests have also been used to determine these moduli (see [8]).

Since the 1990s the rotational stiffness of bolted end connections of pultruded GFRP beams has been the subject of a number of experimental investigations. Most of them have been on mechanically fastened beam-to-column connections. Important early contributions have been reported in [9 – 11] and several state-of-the-art reviews have been published on connections research progress from 1996 up to 2015 (see [12 – 14]).

The present paper presents and discusses both current and new symmetric load tests on simply supported pultruded GFRP beams to determine their elastic flexural moduli. The new test procedure is then used to test similarly loaded beams with bolted joints connected to rigid supports, rather than the flexible flanges or webs of pultruded GFRP columns. Currently, information on the rotational stiffnesses of bolted joints for the former situation is limited. The paper also presents details of the analyses used to evaluate the elastic flexural moduli

and joint rotational stiffnesses from the new test data. The formulae derived from the new analysis are then recast into performance indices for deflection and load for four-point flexure of symmetrically loaded pultruded GFRP beams with semi-rigid end connections, so that the benefits of exploiting the rotational stiffnesses of the beam's end connections can be quantified.

The paper has the following structure. Analyses for determining the elastic flexural moduli from three- and four-point flexure tests on simply supported pultruded GFRP beams are presented first. This is followed by their extension to similarly loaded beams with semi-rigid end connections, in order to provide a means of assessing the benefits of the rotational stiffness of mechanically fastened end connections on the beam's overall flexural stiffness. Thereafter, details of the experimental setups for three- and four-point beam flexure tests and the instrumentation for recording deformations are presented. Following this, the moduli and rotational stiffnesses for both test configurations are compared and contrasted. Thereafter, the new performance indices for the four-point loading configuration are presented and discussed. Finally, the paper is concluded by a summary of the main points arising out of the analysis and test work.

2 Elastic flexural modulus analyses of symmetrically loaded simply supported pultruded GFRP beams

2.1 Three-point loading

Insert Figure 1

Flexural testing of simply supported pultruded GFRP beams has been used to evaluate their elastic flexural and shear moduli by several authors (see [6 & 7]). According to Timoshenko shear deformation beam theory, the mid-span deflection δ_C of the beam shown in Figure 1 subjected to a mid-span point load Q is given as:-

$$\delta_C = \frac{QL^3}{48EI_x} (1 + 12\alpha_x) \quad (1)$$

In Eq.(1) L is the beam's length, E its elastic flexural modulus, I_x its major-axis second moment of area and α_x is its major-axis shear flexibility parameter. The latter is expressed as:-

$$\alpha_x = \frac{EI_x}{GAL^2} \quad (2)$$

In Eq.(2) G is the beam's elastic transverse shear modulus and A its cross-sectional area.

Eq.(1) can be re-arranged to give the elastic flexural modulus E as:-

$$E = \frac{QL^3}{48I_x \delta_C} (1 + 12\alpha_x) \quad (3)$$

It is evident from Eq.(2) that the elastic flexural and transverse shear moduli are present in α_x on the right hand side of Eq.(3). Hence, if the value of the shear modulus G is known, then substituting Eq.(2) into Eq.(3) and re-arranging the following alternative equation for the flexural modulus E is obtained:-

$$E = \frac{QL^3}{48I_x \left(\delta_C - \frac{QL}{4GA} \right)} \quad (4)$$

As both E and G are present in α_x , Eq.(3) cannot be used to determine the value of E from a single three-point flexure test unless $12\alpha_x$ is very small. It is known that α_x reduces as the beam's L/d_s ratio increases, where d_s is the section depth. Therefore, it is of interest to quantify the reduction in $12\alpha_x$ compared to unity as L/d_s increases. In order to do so, the minimum values of the elastic flexural and shear moduli for EXTREN[®] 500 Series Wide Flange (WF) profiles (given in [3]), i.e. 17.93 and 2.93 GPa respectively, together with I_x and A of

a 101.6 x 101.6 x 6.35 mm WF beam are used to calculate α_x for a range of spans L . The section properties of this WF profile were chosen because it features in the test work reported later in the paper. Furthermore, as shear correction factors are not shown explicitly in Eq.(2), the calculations have also been repeated using the web cross-sectional area A_w . The resulting values are denoted as α_{wx} . Corresponding minor-axis calculations have been carried out using I_y , A and A_f (where I_y is the minor-axis second moment of area and A_f is the cross-sectional area of both flanges) to determine the α_y and α_{fy} values for the minor-axis form of Eq.(3). All of the calculations have been carried out for beam spans ranging from 0.25 to 3 m, corresponding to L/d_s ratios ranging from about 2.5 to 30. However, the L/d_s ratios are only presented for $12\alpha_i$ ($i = x, wx, y, fy$) values less than 0.2. The results of these calculations are shown in Figures 2 and 3 for major- and minor-axis three-point flexure, respectively. From Figures 2 and 3 it is evident that, for a given L/d_s ratio, the effect of shear deformation is greater for major- than for minor-axis flexure. Thus, for major-axis flexure, the shear deformation contribution is only less than 5% for L/d_s ratios greater than about 17, whereas for the same effect in minor-axis flexure the L/d_s ratio is about 10.

Insert Figure 2

Insert Figure 3

If Eq.(2) is substituted into Eq.(1), the resulting equation can be re-arranged into the following form:-

$$\frac{\delta_c}{QL} = \frac{L^2}{48EI_x} + \frac{1}{4GA} \quad (5)$$

It is clear from Eq.(5) that a linear relationship exists between δ_c/QL and L^2 , i.e. the slope of the straight line is equal to $1/48EI_x$, from which E can be determined. Moreover, the intercept of the line on the ordinate axis is equal to $1/4GA$. There are, however, two drawbacks to this approach. The first is that the beam has to be tested at several spans (say 5) in order to be able to fit a straight line to the test data. And, secondly, because the straight line fit has to be extended beyond the test data range in order to intersect the ordinate axis, the intercept on the axis will be less accurate than the slope of the line. Hence, the value of the shear modulus will be less accurate than the elastic flexural modulus. That said, Eq.(5) can be re-arranged as:-

$$\frac{\delta_c}{QL^3} = \frac{1}{4GAL^2} + \frac{1}{48EI_x} \quad (6)$$

Hence, plotting δ_c/QL^3 against $1/L^2$ represents a straight line with a slope of $1/4GA$ and an intercept on the ordinate axis of $1/48EI_x$. Therefore, the shear modulus can be determined more accurately from the best-fit straight line to the test data representing Eq.(6).

2.2 Four-point loading

Insert Figure 4

The symmetric four-point flexure test on a simply supported pultruded GFRP beam may also be used to determine the elastic flexural modulus. According to Timoshenko shear deformation beam theory, the mid-span deflection of the beam shown in Figure 4 may be written as:-

$$\delta_c = \frac{QL^3}{96EI_x} (2 - 3\lambda^2 + \lambda^3) \left[1 + 24\alpha_x \frac{(1 - \lambda)}{(2 - 3\lambda^2 + \lambda^3)} \right] \quad (7)$$

In Eq.(7) the symbol λ defines the spacing of the point loads relative to the centre of the span as a fraction of the half-span $L/2$. When the beam is loaded at the quarter span points, then $\lambda = 0.5$ and Eq.(7) becomes:-

$$\delta_c = \frac{11}{768} \frac{QL^3}{EI_x} \left[1 + \frac{96}{11} \alpha_x \right] \quad (8)$$

As before, Eq.(8) can be re-arranged to give an explicit expression for the elastic flexural modulus as follows:-

$$E = \frac{11}{768} \frac{QL^3}{I_x \delta_c} \left[1 + \frac{96}{11} \alpha_x \right] \quad (9)$$

In Eq.(9) the second term in the square brackets represents the contribution of the beam's shear deformation. Furthermore, comparing this term with the corresponding term in Eq.(3), it is evident that the latter term makes a less significant contribution, i.e. $8.727\alpha_x$ compared to $12\alpha_x$. Hence, the L/d_s ratios beyond which shear deformation effects can be ignored are only about three-quarters of those for three-point flexure (see Figures 2 and 3).

Clearly, using Eq.(2), it is possible to re-arrange Eq.(8) as follows:-

$$\frac{\delta_c}{QL} = \frac{11L^2}{768EI_x} + \frac{1}{8GA} \quad (10)$$

so that a plot of δ_c/QL versus L^2 represents a straight line, the slope of which enables the elastic flexural modulus to be determined and the transverse shear modulus may be determined from the intercept of the line on the ordinate axis. However, the disadvantages of adopting this approach are the same as those of the three-point flexure test, namely that tests have to be undertaken for several spans and the intercept on the ordinate axis has to be determined by extrapolating the best-fit straight line beyond the range of the test data. Of course, Eq.(10) can be re-arranged so that the slope of the best-fit straight line through the test data enables the transverse shear modulus to be determined.

2.3 Alternative approach for four-point loading

Insert Figure 5

Insert Figure 6

The bending moment and shear force distributions along the simply supported pultruded GFRP beam subjected to symmetric four-point flexure (see Figure 4) are shown in Figures 5 and 6, respectively. Two features of the central region of the beam D-C-E are of particular importance to the development of the alternative method of determining the beam's elastic flexural modulus. The first is that the shear force is zero. Consequently, shear has no effect on the flexure of the central region of the beam. The second is that the bending moment is uniform over the same region, so that it is in a state of symmetric pure bending. Hence, providing the deformation of the beam remains within the linear regime, the following equations for the longitudinal strain ϵ_x and bending moment M_x apply:-

$$\epsilon_x = -\frac{z}{\rho_x} \quad (11)$$

$$M_x = \frac{EI_x}{\rho_x} \quad (12)$$

In Eqs.(11) and (12) z is the distance above the major-axis of the cross-section where the strain ϵ_x is recorded and ρ_x is the radius of curvature at that cross-section.

Because of the symmetry of the loading, the deflected shape of the beam between the loading points D and E is also symmetric. Hence, the deflection at C, δ_c , may be expressed in terms of the radius of circular curvature ρ_{xc} at C and the gauge length d between two symmetric points either side of C. This relationship is:-

$$\delta_C = \frac{d^2}{8\rho_{xc}} \quad (13)$$

Now replacing $-z$ in Eq.(11) with $d/2$ and setting $\varepsilon_x = \varepsilon_{xc}$ (the strain at C) and then substituting the resulting equation together with Eq.(13) into Eq.(12) and re-arranging, the following three equations for computing the longitudinal elastic flexural modulus are obtained:-

$$E = \frac{M_x d_s}{2I_x \varepsilon_{xc}} = \frac{M_x \rho_{xc}}{I_x} = \frac{M_x d^2}{8I_x \delta_C} \quad (14)$$

Hence, substituting the expression for M_x in terms of the applied loads $Q/2$ (see Figure 5) Eqs.(14) become:-

$$E = \frac{QL(1-\lambda)d_s}{8I_x \varepsilon_x} = \frac{QL(1-\lambda)\rho_{xc}}{4I_x} = \frac{QL(1-\lambda)d^2}{32I_x \delta_C} \quad (15)$$

It is evident from Eqs.(15) that the longitudinal elastic flexural modulus can be determined from Q together with ε_{xc} or ρ_{xc} or δ_C and the gauge length d . A curvature meter is required for the latter two approaches, a schematic diagram of which is shown in Figure 7(a) alongside the actual adjustable meter in Figure 7(b).

Insert Figure 7 (a)

Insert Figure 7 (b)

3 Analysis of the rotational stiffness of the semi-rigid supports of a pultruded GFRP beam subjected symmetric four-point loading

Figure 8 shows a schematic diagram of a single-span pultruded GFRP beam with semi-rigid supports at A and B. It is assumed that the rotational stiffness of each semi-rigid support is K .

Insert Figure 8

The analysis of this redundant structural system can be reduced to the superposition of two sub-systems, referred to as Systems I and II. System I is the simply supported beam subjected to the four-point loading shown in Figure 4 and System II is the same beam loaded by equal and opposite end moments M , due to the rotational restraint provided by the semi-rigid end connections, as shown in Figure 9.

Insert Figure 9

Assuming that the beam in Figure 8 is in a state of major-axis flexure, its mid-span deflection δ_C and its end rotations θ_A and θ_B can be obtained by adding the corresponding displacements of Systems I and II, as follows:-

System I

$$\delta_C^I = \frac{QL^3}{96EI_x} \left[(2-3\lambda^2 + \lambda^3) + 24\alpha_x (1-\lambda) \right] \quad (7a)$$

$$\theta'_A = \frac{QL^2}{16EI_x}(1-\lambda^2) = -\theta'_B \quad (16)$$

System II

$$\delta''_C = \frac{ML^2}{8EI_x} \quad (17)$$

$$\theta''_A = \frac{ML}{2EI_x} = -\theta''_B \quad (18)$$

Hence, the mid-span deflection δ_C is obtained by subtracting Eq.(17) from Eq.(7a), as follows:-

$$\delta_C = \delta'_C - \delta''_C = \frac{QL^3}{96EI_x} \left[(2-3\lambda^2 + \lambda^3) + 24\alpha_x(1-\lambda) \right] - \frac{ML^2}{8EI_x} \quad (19)$$

Likewise, subtracting Eq.(18) from Eq.(16) gives:-

$$\theta_A = \theta'_A - \theta''_A = \frac{QL^2}{16EI_x}(1-\lambda^2) - \frac{ML}{2EI_x} = -\theta_B \quad (20)$$

Now, if the rotational stiffness of the semi-rigid support at A and B is K, then M can be expressed as:-

$$M = K\theta_A \quad (21)$$

Hence, substituting Eq.(21) into Eq.(20) and defining the rotational flexibility β of the semi-rigid joints as:-

$$\beta = \frac{EI_x}{KL} \quad (22)$$

then θ_A may be re-arranged to give:-

$$\theta_A = \frac{QL^2}{8EI_x} \frac{(1-\lambda^2)\beta}{(1+2\beta)} \quad (23)$$

Now substituting Eq.(23) into Eq.(21) the moment M at the semi-rigid end connections may be written as:-

$$M = \frac{QL}{8} \frac{(1-\lambda^2)}{(1+2\beta)} \quad (24)$$

Furthermore, substituting Eq.(24) into Eq.(19) gives an alternative equation for the mid-span deflection δ_C as:-

$$\delta_C = \frac{QL^3}{96EI_x} \left[(2-3\lambda^2 + \lambda^3) + 24\alpha_x(1-\lambda) - \frac{3(1-\lambda^2)}{2(1+2\beta)} \right] \quad (25)$$

Hence, substituting Eq.(22) into Eq.(25) and re-arranging the result, the following formula for the rotational stiffness K of the semi-rigid joint may be derived:-

$$K = \frac{2 \frac{EI_x}{L}}{\left[\frac{\frac{3}{2}(1-\lambda)^2}{(2-3\lambda^2+\lambda^3)+24\alpha_x(1-\lambda)+96\frac{EI_x}{L^3}\frac{\delta_c}{Q}} - 1 \right]} \quad (26)$$

The mid-span bending moment M_C can be expressed as:-

$$M_C = \frac{QL}{4}(1-\lambda) - M \quad (27)$$

Hence, from Eqs.(11) and (12) the strain ε_{xc} at the outer surface of the beam's compression flange may be expressed as:-

$$\varepsilon_{xc} = M_C \frac{d_s}{2EI_x} \quad (28)$$

and substituting Eq.(28) into Eq.(27), the moment M at the semi-rigid support can be expressed as:-

$$M = \frac{QL}{4}(1-\lambda) - 2 \frac{EI_x}{d_s} \varepsilon_{xc} \quad (29)$$

Now, substituting Eq.(24) into Eq.(29), the following alternative expression for the rotational stiffness of the semi-rigid joint may be derived:-

$$K = \frac{2 \frac{EI_x}{L}}{\left[\frac{(1-\lambda^2)}{\left\{ 2(1-\lambda) - 16 \frac{EI_x}{Ld_s} \frac{\varepsilon_{xc}}{Q} \right\}} - 1 \right]} \quad (30)$$

Furthermore, if a curvature meter is used (see Figure 9), then from Eqs.(11) and (13) ε_{xc} may be expressed as:-

$$\varepsilon_{xc} = 2 \frac{d_s s}{d^2} \quad (31)$$

Hence, substituting Eq.(31) into Eq.(30) the following alternative equation for the rotational stiffness of the semi-rigid end connections is obtained as:-

$$K = \frac{2 \frac{EI_x}{L}}{\left[\frac{(1-\lambda^2)}{\left\{ 2(1-\lambda) - 32 \frac{EI_x}{Ld^2} \frac{s}{Q} \right\}} - 1 \right]} \quad (32)$$

4 Alternative three- and four-point pultruded GFRP beam tests incorporating a curvature meter and strain gauges

4.1 Simply supported beam tests to determine the longitudinal elastic modulus

A 101.6 x 101.6 x 6.35 mm WF EXTREN[®] 500 series pultruded GFRP profile was selected for the simply supported beam flexure tests from which the longitudinal elastic moduli were to be determined. The beams were to be loaded in both three- and four-point major- and minor-axis flexure for a range of spans. Details of their section properties are given in Table 1.

Insert Table 1

The three-point major- and minor-axis tests were carried out on WF profiles of overall length 2.6 m with a test span of 2.52 m. Two WF profiles of overall lengths 2.6 m and 2 m were selected for the four point major- and minor-axis tests. The simply supported spans of the 2.6 m long profile were 2.4 m and 2 m and for the 2 m profile its simply supported span was 1.6 m.

4.1.1 Support and loading setups for the three- and four-point simply supported beam tests

For the major-axis tests the beam ends were supported on a 38 mm diameter solid steel rod in contact with the lower flange, as shown in Figure 10(a). However, a different arrangement was adopted for the minor-axis tests. A 25 mm long steel *shoe* was placed between each flange edge and the steel knife edge support in order to prevent the knife edge indenting the flange edge and causing rotational restraint at the support. This arrangement is illustrated in Figure 10(b).

Insert Figure 10 (a)

Insert Figure 10 (b)

Just as different end support arrangements were used for the major- and minor-axis flexure tests, so different means of loading the beams had to be adopted for each axis of flexure. The major-axis loading arrangement is shown in Figure 11(a). In this arrangement a 19 mm diameter solid steel rod welded to a 75 x 40 mm steel plate is between the upper flange of the beam and the horizontal upper bar of the load hanger. There is a 1 mm thick rubber pad between the steel plate and the upper flange to spread the load.

Insert Figure 11 (a)

Insert Figure 11 (b)

In the minor-axis loading arrangement, shown in Figure 11(b), the load from the upper horizontal bar of the load hanger is transferred via a steel ball bearing to a 22 x 22 mm cross-section steel bar on top of the 25 mm long steel *shoes* on top of the upper edges of the beam's flanges.

For the three-point flexure tests a single load hanger, positioned at mid-span, was used. The load was applied by a jack pulling down on the lower horizontal bar of the load hanger. On the other hand, for the four-point flexure tests two load hangers, located at the quarter-span positions, were used. Their lower horizontal bars were connected by a horizontal steel beam. A single tension jack connected to the centre of the steel beam was used to apply the two equal point loads.

The total applied load was measured by a 10 kN capacity load cell with a 10 N load resolution. In the three-point flexure tests the load cell was connected between the ram of the jack and the lower horizontal bar of the load hanger, and in the four-point flexure tests the load cell was between the jack's ram and the centre of the horizontal steel beam.

4.1.2 Instrumentation and loading procedure

In the major-axis tests (both three- and four-point) the centre deflection was recorded by a dial gauge with a 45 mm travel and a displacement resolution of 0.01 mm in contact with the centre of the lower flange. However, for the minor-axis tests the centre deflection was recorded with the same dial gauge in contact with the centre of the web.

In most of the four-point major-axis tests a single strain gauge (120 Ohms internal resistance and 10 mm gauge length) with its sensitive axis aligned with the beam's longitudinal axis was used to record the outer surface compressive strain of the upper flange. Likewise, a uniaxial strain gauge was bonded to the lower flange edge for the majority of the minor-axis tests. For the shortest span tests an additional strain gauge was used to monitor the corresponding lower flange/flange edge tensile strain.

The curvature meter (see Figure 7) was also used in the four-point flexure tests to monitor the mid-span curvature.

Depending on the span, the beams were loaded in equal increments ranging from 250 – 750 N (major-axis flexure) and from 100 – 300 N (minor-axis flexure) up to maximum deflections of about 30 mm and the corresponding loads, deflections, strains and curvatures were recorded. A 12 hour recovery period was allowed between each of the three- and four-point flexure tests.

4.1.3 Elastic moduli obtained from the deflection, curvature and strain measurements

Using the beam cross-section details from Table 1 together with the relevant load, deflection, strain and curvature data for each of the three- and four-point major- and minor-axis tests the longitudinal elastic modulus E was calculated for each span L using the relevant forms of Eqs.(3) and (15). The modulus values are presented in Table 2.

The values of the longitudinal elastic moduli presented in Table 2 exclude the effect of shear deformation. As shown earlier, the effects of shear deformation are greater for the three-point than the four-point flexure tests. It is of interest to estimate the effects of shear deformation for these tests. This may be carried out using the data presented in Figures 2 and 3, by estimating the values of the shear flexibility factors $12\alpha_i$ ($i = x, wx, y$ and fy) corresponding to the L/d_s ratios of the test spans. The approximate values of these factors are presented in Table 3.

Insert Table 2

Insert Table 3

The load – deflection responses obtained from the major- and minor-axis tests on the 2.52 m span simply supported pultruded GFRP beam subjected to symmetric three- and four-point flexure are shown together with the corresponding theoretical responses in sub-section 4.2.3 as part of the load – deflection responses obtained from the three- and four-point flexure tests on beams with semi-rigid end connections.

4.2 Beam tests to determine the rotational stiffnesses of the semi-rigid end connections

4.2.1 Bolted end connection details

A pultruded GFRP beam was prepared for testing with semi-rigid end connections from the 2.6 m overall length of WF profile used in the simply supported beam tests. The semi-rigid end connections were created using cleats cut out of a 101.6 x 101.6 x 9.5 mm EXTREN® 500 Series angle profile. Three types of bolted end connection were fabricated, namely web, flange and web and flange. The connections used 10 mm diameter bolts with long smooth shanks in order to avoid thread contact with the bolt holes. The bolts were torqued to 35 Nm. There were two bolts in each leg of the flange cleats, two bolts in the leg of the web cleats connected to the beam's web and only one bolt in the leg connected to the rigid steel support.

Insert Figure 12

A dimensioned drawing of the web and flange cleat connection is shown in Figure 12. The dimensions of the flange and web cleat connections were similar to those shown in Figure 12, but with the respective web or flange cleats removed. An image of the bolted web and flange end connection used in the minor-axis semi-rigid beam tests is shown in Figure 13.

Insert Figure 13

The rigid end support to which the GFRP angle cleats were bolted was provided by a welded, mild steel, gusseted angle, the vertical and horizontal legs of which were 20 mm thick. An image of the gusseted angle is shown in Figure 14. Two electronic clinometers were attached to the rear of the vertical leg and the inside face of one gusset plate in order to detect any flexibility of the *rigid* support during the three- and four-point flexure tests. As expected, the clinometers did not register any changes to their zero load readings, thereby confirming that the gusseted steel angles behaved as rigid supports.

Insert Figure 14

4.2.2 Experimental setup for the four-point flexure tests

In order to achieve the same span as that used in the simply supported beam tests, i.e. 2.52 m, the beam was shortened to 2.43 m, so that when the GFRP angle cleats were bolted to it, its overall span was 2.52 m. An overall view of the test setup, which shows a four-point minor-axis flexure test on a beam with bolted flange cleat end connections is shown in Figure 15.

Insert Figure 15

4.2.3 Rotational stiffnesses of the bolted end connections obtained from the three- and four-point flexure tests

As for the earlier simply supported beam tests, the beams were loaded incrementally up to maximum loads of about 5 - 6 kN and 2 - 2.5 kN for the major- and minor-axis three-point flexure tests, respectively. The corresponding maximum loads for the major- and minor-axis four-point flexure tests were about 7 - 8 kN and 2.5 - 3.5 kN, respectively. During each test loads, deflections, strains and curvatures were recorded after the application of each load increment. Two to four repeat tests were carried out for each major- and minor-axis and end connection configuration and 12 hour recovery periods were allowed between each successive load - deflection test.

Using data, i.e. loads and corresponding mid-span deflections, curvatures and strains, obtained from the three- and four-point major- and minor-axis flexure tests on the beams and substituting the data, together with mean elastic moduli obtained from the respective simply supported beam tests, into Eqs.(26), (30) and (32) the rotational stiffnesses of the bolted angle cleat connections were calculated. The values of these stiffnesses are presented in Table 4.

Insert Table 4

Problems with failure of the GFRP angle cleats arose during the four-point flexure tests on beams with bolted flange cleat end connections. Nevertheless, for the most part the rotational stiffnesses obtained for the bolted web and flange and flange cleat connections appear to be reasonably consistent for both the three- and four-point flexure tests. On the other hand, there is rather more variation in the major-axis rotational stiffnesses of the more flexible web cleat connections obtained from the three- and four-point flexure tests. The only other test data available for comparison with the present end connection rotational stiffnesses is that reported in [15]. It is evident that there is reasonably good agreement for the mean major-axis rotational stiffnesses of the web connection, but for the web and flange cleat connection, the rotational stiffness reported in [15] is significantly higher than the present mean rotational stiffness.

In Figure 16 the experimental load - mid-span deflection graphs are presented for the three- and four-point flexure tests. Superimposed on the experimental results are the corresponding theoretical full-line responses. Also shown in Figure 16 are the experimental and theoretical load - deflection responses obtained from the

three- and four-point flexure tests on the simply supported beams. It is evident that there is good agreement between theoretical and tests results in all cases.

Insert Figure 16 (a)

Insert Figure 16 (b)

Insert Figure 16 (c)

Insert Figure 16 (d)

5 Serviceability limit loads of pultruded GFRP beams subjected to symmetric four-point flexure

As pointed out earlier, the deflection serviceability limit generally governs the design of pultruded GFRP beams and dictates the loads they are able to carry. The most recent *code-like* design guidance documents [1 & 2] do not provide very specific guidance on what the deflection limits should be for different design situations. However, Table 4.2 of the EUROCOMP Design Code and Handbook [16] does provide guidance for a number of design situations. The deflection limits are specified in terms of fractions of the beam span:-

$$\delta_c = \frac{L}{k} \quad (33)$$

In Eq.(33) δ_c is the maximum deflection at mid-span, L is the beam span and k is a number which depends on the design situation. For the most sensitive deflection situation $k = 400$, for the least sensitive situation $k = 150$ and for the *general public access* situation $k = 250$.

It is of interest to quantify the serviceability limit loads and see how they vary in accordance with the rotational stiffness of the beams' end connections. This may be accomplished by re-arranging Eq.(25) as follows,

$$Q = \frac{\left(\frac{1}{k}\right)\left(\frac{96EI_x}{L^2}\right)}{\left[(2 - 3\lambda^2 + \lambda^3) + 24\alpha_x(1 - \lambda) - \frac{3(1 - \lambda^2)}{2(1 + 2\beta)} \right]} \quad (34)$$

In Eq. (34) Q is the load corresponding to the deflection serviceability limit. Hence, substituting into Eq.(34) the values for E, I_x , L, α_x and β the major-axis serviceability limit loads may be calculated for the practical range of span to depth ratios (L/d_c) for $k = 250$ for each of the three types of bolted end connection. The results of these calculations are in Figure 17.

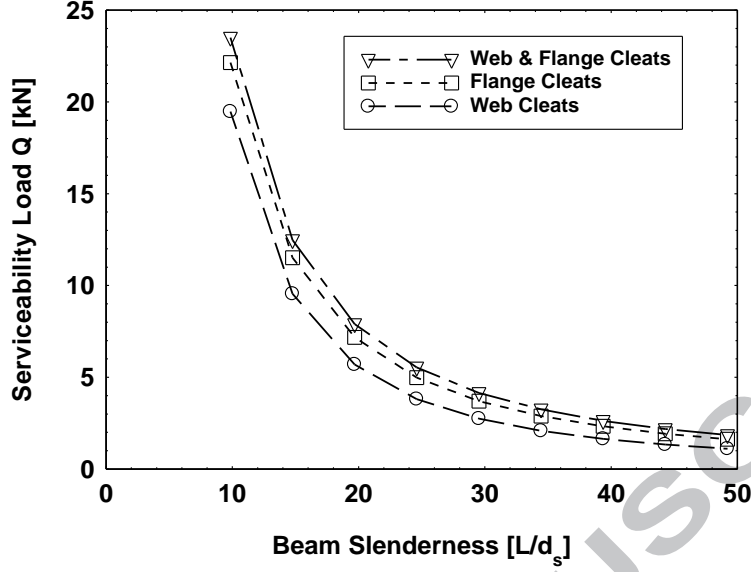


Figure 17: Serviceability load versus beam slenderness for a pultruded GFRP 101.6 x 101.6 x 6.35 mm WF beam with three types of bolted end connections and subjected to four-point flexure [$k = 250$]

As expected, it is clear that serviceability loads reduce significantly as the beam slenderness increases. It is also evident that substituting flange connections for web connections produces a larger increase in the serviceability load than adding web cleats to a beam with flange cleat end connections. Furthermore, the serviceability limit loads for the more and less stringent k -values, i.e. $k = 400$ and 150 , are obtained by multiplying the loads in Figure 17 by 0.625 and 1.667 , respectively.

6 Performance indices for deflection and load for pultruded GFRP beams subjected to symmetric four-point flexure

The concept of performance indices for single-span pultruded GFRP beams subjected to mid-span point loading or uniformly distributed loading over the entire span was introduced in the late 1990s (see [15 & 17]). The purpose of these indices was to provide a simple means of assessing the benefits of semi-rigid end connection stiffnesses in reducing the mid-span deflection and increasing the load capacity relative to an otherwise identically loaded simply supported beam. As part of the investigation reported herein, corresponding performance indices have been derived for the general case of symmetric four-point flexure.

Eq.(25) in Section 3 gives a general expression for the major-axis mid-span deflection of a pultruded GFRP beam with semi-rigid end connections when subjected to symmetric four-point loading (see Figure 8). This equation can be re-arranged into the following, more convenient form for the development of performance indices:-

$$\delta_c = \frac{QL^3(1-\lambda)}{192EI_x} \left[\frac{(1-\lambda)(1+2\lambda) + 48\alpha_x + 4\beta(2+2\lambda-\lambda^2) + 96\alpha_x\beta}{(1+2\beta)} \right] \quad (35)$$

If now the beam is assumed to have simply supported rather than semi-rigid ends, then the beam's rotational flexibility $\beta = \infty$ and Eq.(35) simplifies to:-

$$\delta_c = \frac{QL^3(1-\lambda)}{96EI_x} \left[(2+2\lambda-\lambda^2) + 24\alpha_x \right] \quad (36)$$

Now, if it is assumed that the elastic and geometric properties of the simply supported and semi-rigidly supported beams are identical and that both beams carry the same total load, then the ratio of their mid-span deflections λ_s is obtained by dividing Eq.(35) by Eq.(36), so that:-

$$\lambda_{\delta} = \frac{\left[(1-\lambda)(1+2\lambda) + 48\alpha_x + 4\beta(2+2\lambda-\lambda^2) + 96\alpha_x\beta \right]}{\left[2(2+2\lambda-\lambda^2) + 48\alpha_x + 4\beta(2+2\lambda-\lambda^2) + 96\alpha_x\beta \right]} \quad (37)$$

Furthermore, if the end conditions of the semi-rigidly supported beam are changed to clamped, i.e. $\beta = 0$, then Eq.(37) reduces to:-

$$\lambda_{\delta} = \frac{\left[(1-\lambda)(1+2\lambda) + 48\alpha_x \right]}{\left[2(2+2\lambda-\lambda^2) + 48\alpha_x \right]} \quad (38)$$

Now if the clamped and simply supported beams are shear-rigid, i.e. $\alpha_x = 0$, then Eq.(38) reduces to:-

$$\lambda_{\delta} = \frac{\left[(1-\lambda)(1+2\lambda) \right]}{\left[2(2+2\lambda-\lambda^2) \right]} \quad (39)$$

From Figure 4, it is evident that the lower and upper bound values of λ are 0 and 1. The latter value corresponds to both beams being unloaded, so that the mid-span deflection ratio $\lambda_{\delta} = 0$, and the former value corresponds to both beams supporting the same load Q at mid-span with the mid-span deflection ratio $\lambda_{\delta} = 0.25$. This result has been demonstrated previously in [15].

It is of interest to evaluate the deflection performance indices for four-point major- and minor-axis flexure using the mean rotational stiffnesses given in Table 4 for the 101.6 x 101.6 x 6.35 mm WF beam. The indices for major- and minor-axis flexure, respectively, are shown in Figure 18. The shear flexibility parameter α_x used to calculate the data points in Figure 18(a) was based on the gross cross-sectional of WF beam and no shear correction factor was used. In fact data points using α_x -values based on web cross-sectional area (for major-axis flexure) and α_y -values based on flange cross-sectional area (for minor-axis flexure) as well as $\alpha_{x,y} = 0$ were also calculated. However, for the beam span of 2.4 m the differences between the latter values and those obtained using the gross cross-sectional area were negligible.

Insert Figure 18 (a)

Insert Figure 18 (b)

It is evident that for both major- and minor-axis four-point flexure the deflection performance index is almost independent of the positions of the point loads on the span for beams with bolted web cleat connections at their ends. Furthermore, the web cleat connections provide less than 20% reduction in mid-span deflection. As expected, the bolted web and flange cleat connections provide the maximum reduction in mid-span deflection and the reduction increases as the separation between the two point loads increases. However, the deflection reduction effect is greater for minor-axis than for major-axis flexure. For the former case it ranges from 50% to 64% and for the latter case from 38% to 49%. Also, the flange cleat connections for minor-axis flexure produce a greater reduction in mid-span deflection than the web and flange joints for major-axis flexure.

Now the load performance index, denoted as λ_Q , is obtained by assuming equal mid-span deflections as well as equal material and geometric properties when comparing Eqs.(35) and (36). It is, therefore, obvious that λ_Q is simply the inverse of λ_{δ} . Hence, the load performance index is:-

$$\lambda_Q = \frac{1}{\lambda_{\delta}} \quad (40)$$

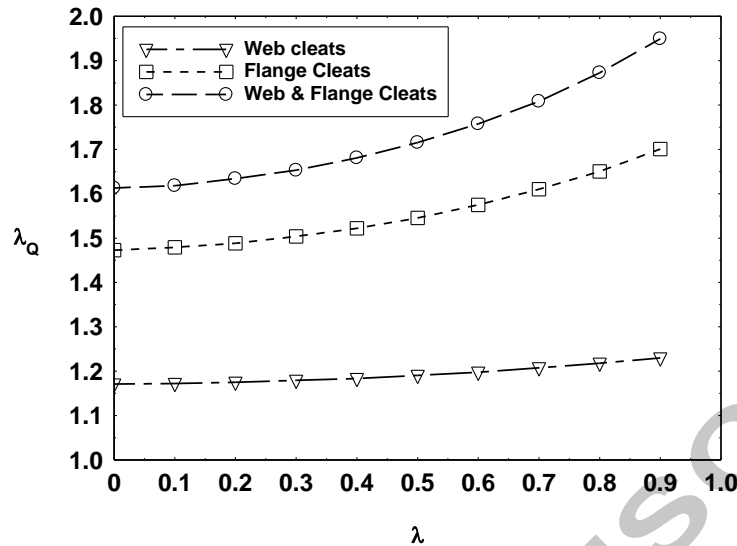


Figure 19: Load performance index versus load spacing ratio for four-point major-axis flexure of a 101 x 101 x 6.35 mm pultruded GFRP WF beam with semi-rigid end connections

The values used to plot the graphs in Figure 19 are the inverse of those used to plot Figure 18(a). It should be appreciated the data points on the λ_Q -axis correspond to the loads for the beam subjected to symmetric three-point flexure for the three types of bolted end connections. As the positions of the loads are moved progressively towards the end connections, the magnitudes of the loads increase. Comparing the values for $\lambda = 0.9$ with those for $\lambda = 0$, it is evident that for web cleat end connections the increase in the load is about 5%, whereas for flange and web and flange cleat end connections the corresponding increases are approximately 15% and 21% respectively.

A third performance index, namely the span performance index, λ_L , may also be established. However, as this is of limited interest and does not result in an explicit expression for the index it will not be considered further here.

6 Concluding remarks

Previous test methods and their associated analyses used to determine the longitudinal elastic flexural moduli of pultruded GFRP beams have been reviewed. New three- and four-point simply supported beam flexure tests and analyses based on mid-span deflection, strain and curvature data are described. A novel feature is an adjustable curvature meter. The new tests and analyses have been shown to yield consistent values for the longitudinal elastic flexural modulus of a simply supported 101.6 x 101.6 x 6.35 mm WF beam subjected to symmetric three- and four-point flexure.

The experimental approach, i.e. simultaneous mid-span deflection, strain and curvature monitoring, together with the relevant analytical developments, has been extended to single-span GFRP beams with three types of semi-rigid end connection, i.e. bolted web, flange, and web and flange cleat connections. The theoretical analysis has been verified experimentally for WF beams subjected to symmetric three- and four-point flexure and consistent rotational stiffnesses have been obtained for the connections.

The semi-rigid symmetric four-point flexural analysis has been reformulated to compute loads corresponding to specific limit state deflection serviceability criteria. Loads have been presented as a function of beam slenderness for the general deflection limit state criterion for the three types of end connection.

Finally, the equation for the mid-span deflection of a shear-deformable pultruded GFRP beam with semi-rigid end connections has been re-arranged and compared to the corresponding equation for a simply supported beam to obtain performance indices for mid-span deflection and load. The deflection performance indices have been evaluated for major- and minor-axis flexure for a range of load spacings for the three types of bolted end connection. It has been shown that web and flange cleat connections reduce mid-span deflections by 38% to

49% for major-axis loading and 50% to 64% for minor-axis loading. For bolted web connections the reduction in mid-span deflection was between 17% and 21%, i.e. not very sensitive to the load spacing on the beam.

For major-axis four-point flexure the load performance indices revealed maximum load increases of 5%, 15% and 21% for web, flange and web and flange connections, respectively compared to the case of three-point mid-span flexural loading.

Acknowledgements

The test work and the majority of the analysis, reported herein, was completed as part of a three-year research programme funded by EPSRC (Grant GR/R28386). The authors wish to record their appreciation to EPSRC for supporting their research. They also wish to acknowledge the help and assistance given by the Engineering Department's technician staff.

References

- 1 Anon. *Pre-Standard for Load and Resistance Factor Design (LRFD) of Pultruded Fiber Reinforced Polymer (FRP) Structures*, American Society of Civil Engineers, Reston, Virginia, USA, 2010.
- 2 Ascione. L. et. al. *Prospect for New Guidance in the Design of FRP*, JRC Science and Policy Report (JRC99714, EUR 27666 EN, European Union, Luxembourg, 2016.
- 3 Anon. *EXTREN Design Manual*, Strongwell, Bristol, Virginia, USA (<http://www.strongwell.com>) [accessed: 4-10-2017].
- 4 Anon. *Creative Pultrusions Design Guide*, Creative Pultrusions Incorporated, Alum Bank, Pennsylvania, USA. (<http://www.creative.com>) [accessed: 4-10-2017].
- 5 Anon. *Design Guide*, Bedford Reinforced Plastics, Bedford, Pennsylvania, USA. (<http://www.bedfordreinforced.com>) [accessed: 4-10-2017].
- 6 Sims GD, Johnson AF and Hill R. Mechanical and structural properties of a GFRP pultruded section. *Composite Structures*, 1987;8(3):173-187.
- 7 Bank LC. Flexural and shear moduli of full-section fibre reinforced plastic (FRP) pultruded beams. *ASTM Journal of Testing and Evaluation* 1989;17(1):40-45.
- 8 Minghini F, Tullini N and Laudiero F. Identification of the short-term full-section moduli of pultruded FRP profiles using bending tests. *Journal of Composites for Construction*, 2014;18(1):04013030.
- 9 Turvey GJ and Cooper C. Characterisation of the short term static moment - rotation response of bolted connections between pultruded GRP beam and column WF-sections. Proceedings of the 2nd International Conference on Advanced Composite Materials in Bridges and Structures (ACMBS II), 11th-14th August, 1996, Montreal. Published in *Advanced Composite Materials in Bridges and Structures*, Edited by M. El-Badry, Canadian Society for Civil Engineering, Montreal, (1996), 927-934.
- 10 Mottram JT and Zheng Y. Further tests on beam-to-column connections for pultruded frames: web-cleated. *Journal of Composites for Construction*, 1999;3(1):3-11.
- 11 Mottram JT and Zheng Y. Further tests on beam-to-column connections for pultruded frames: flange-cleated. *Journal of Composites for Construction*, 1999;3(3):108-116.
- 12 Mottram JT and Zheng Y. State-of-the-art review on the design of beam-to-column connections for pultruded frames. *Composite Structures*, 1996;35(4):387-401.
- 13 Turvey, GJ and Cooper C. Review of tests on bolted joints between pultruded GRP profiles. *Proceedings of the Institution of Civil Engineers: Structures and Buildings*, 2004;157 (3):211-233.
- 14 Girao Coelho AM and Mottram JT. A review of the behaviour and analysis of mechanically fastened joints in pultruded fibre reinforced polymers. *Materials and Design*, 2015;74:86-107.
- 15 Turvey GJ. Analysis of pultruded glass reinforced plastic beams with semi-rigid end connections. *Composite Structures*, 1997;38(1-4):3-16.
- 16 Clarke JL (Ed.). *EUROCOMP Design Code and Handbook*, E & FN Spon, London, 1996.
- 17 Turvey GJ. Flexure of pultruded GRP beams with semi-rigid end connections. *Composite Structures*, 1999;47:571-580.

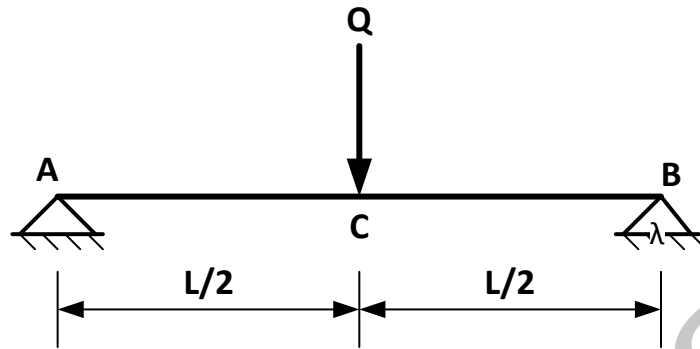


Figure 1: A simply supported pultruded GFRP beam subjected to symmetric three-point major-axis flexure

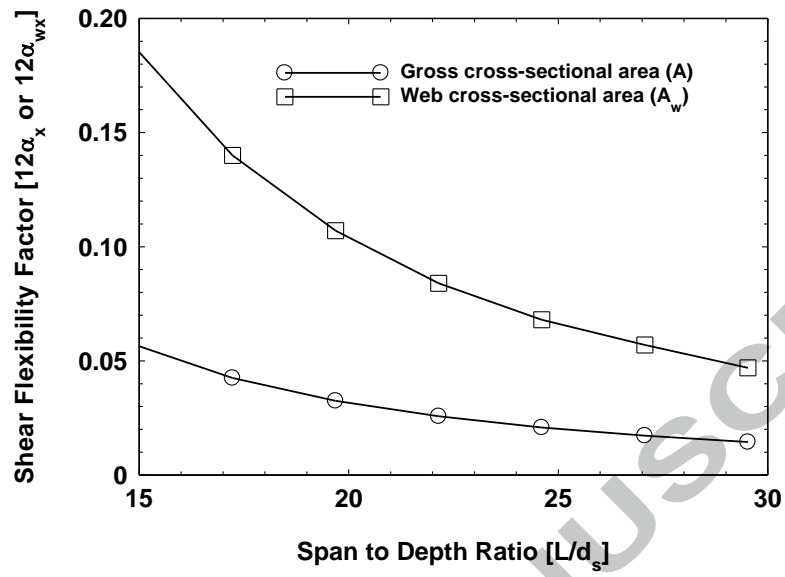


Figure 2: Reduction in the shear deformation contribution to the overall mid-span deflection with increasing span to depth ratio for three-point flexure of a pultruded GFRP 101 x 101 x 6.35 mm WF beam (major-axis flexure)

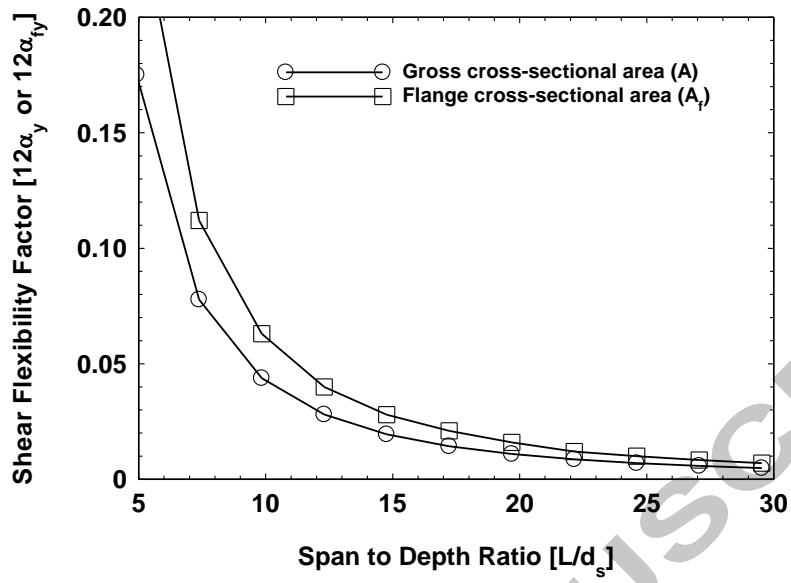


Figure 3: Reduction in the shear deformation contribution to the overall mid-span deflection with increasing span to depth ratio for three-point flexure of a pultruded GFRP 101 x 101 x 6.35 mm WF beam (minor-axis flexure)

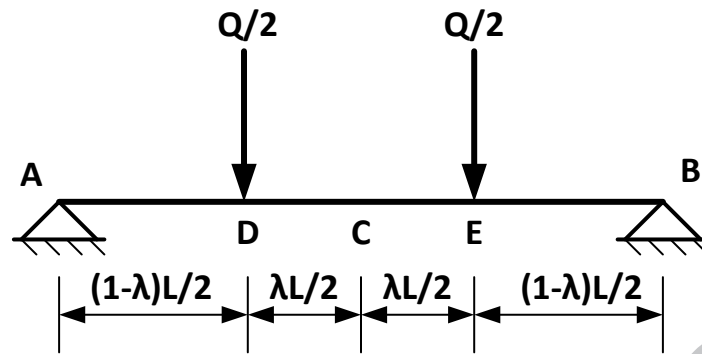


Figure 4: A simply supported pultruded GFRP beam subjected to symmetric four-point flexure [referred to later as System I]

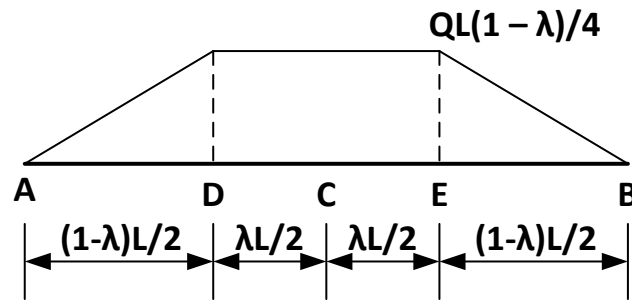


Figure 5: Bending moment distribution along the simply supported pultruded GFRP beam subjected to symmetric four-point loading

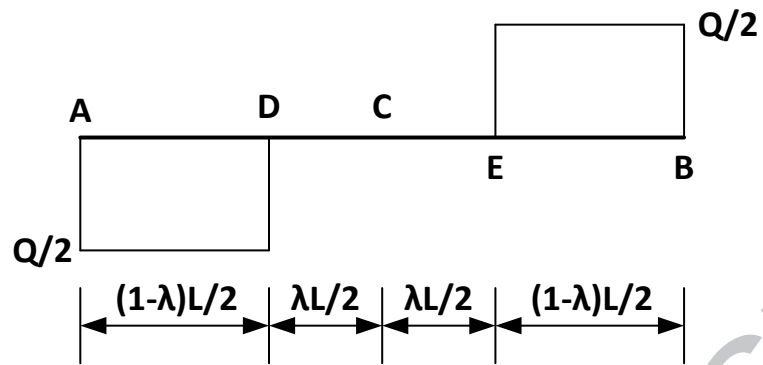


Figure 6: Shear force distribution along the simply supported pultruded GFRP beam subjected to symmetric four-point loading

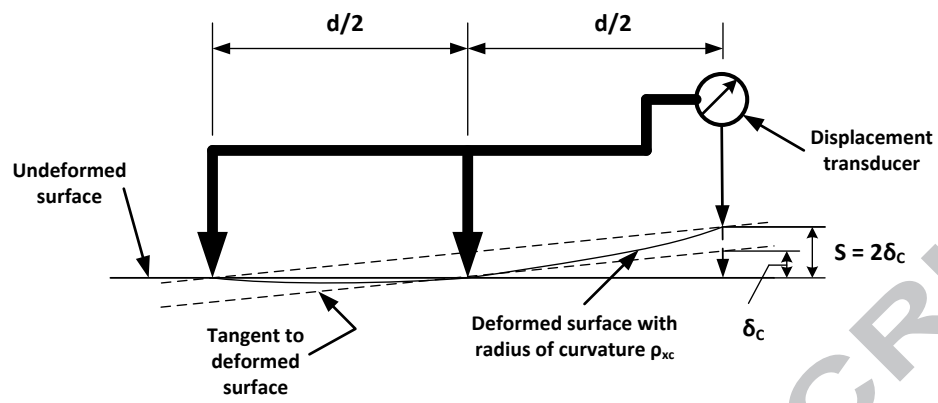


Figure 7(a): Curvature meter (schematic diagram)



Figure 7(b): variable gauge length meter

ACCEPTED MANUSCRIPT

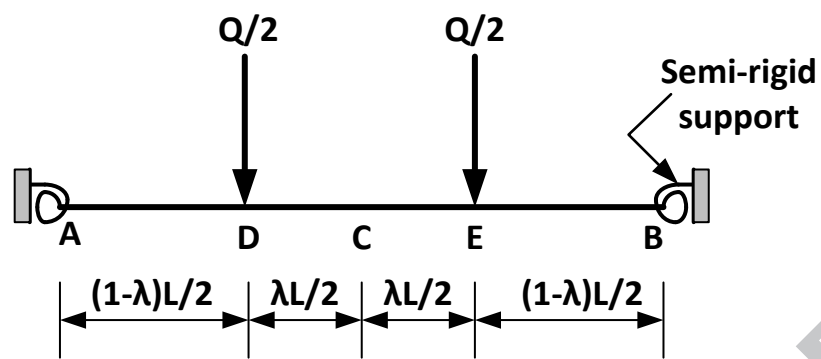


Figure 8: A pultruded GFRP beam with semi-rigid end supports subjected to symmetric four-point loading

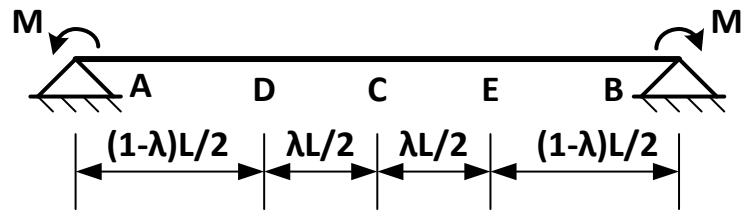


Figure 9: A simply supported pultruded GFRP beam subjected to equal and opposite moments M at its ends A and B [System II]

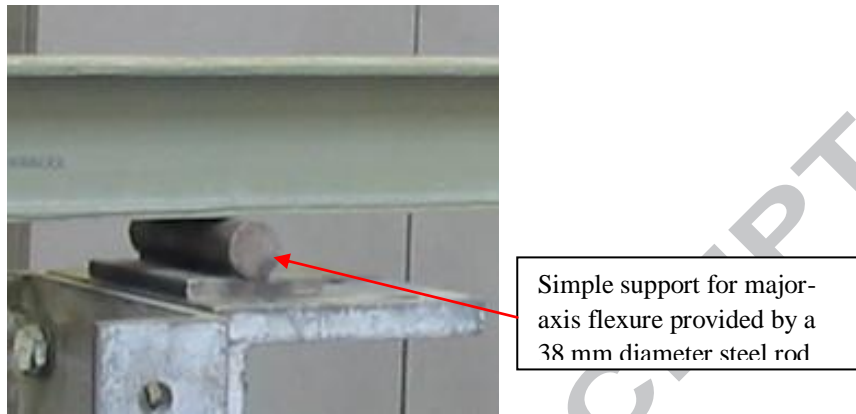


Figure 10 (a)

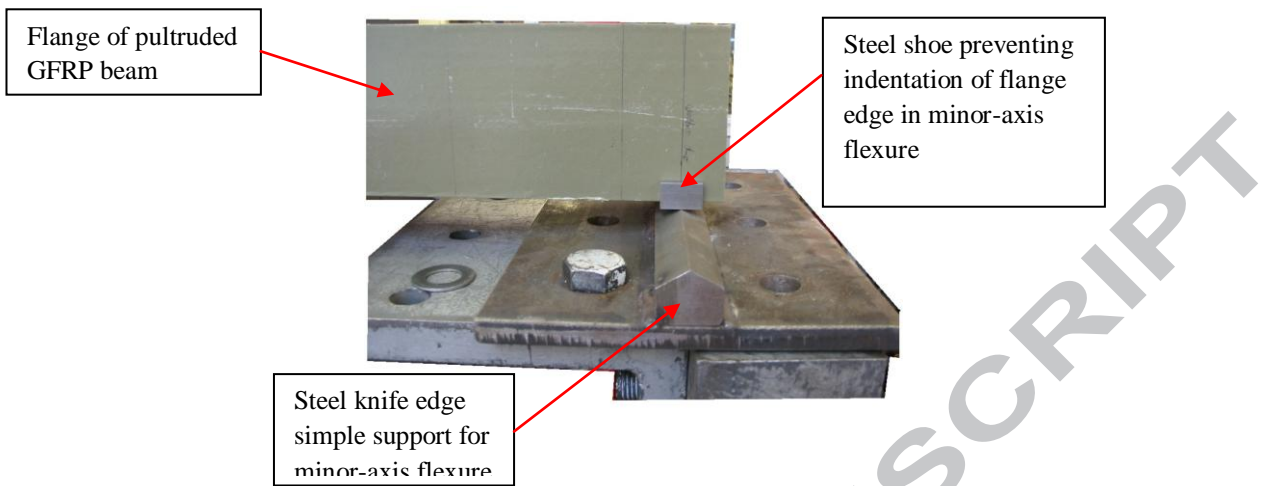


Figure 10(b)

ACCEPTED MANUSCRIPT

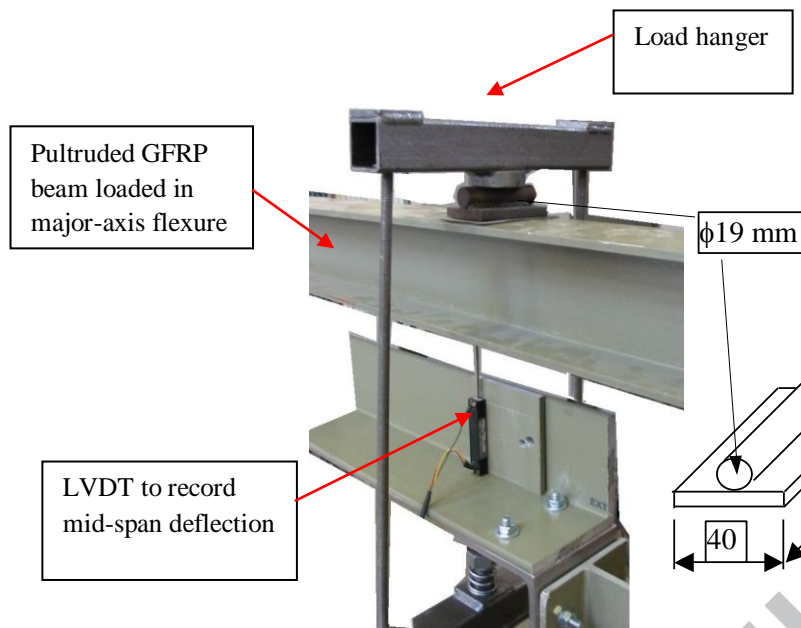


Figure 11(a)

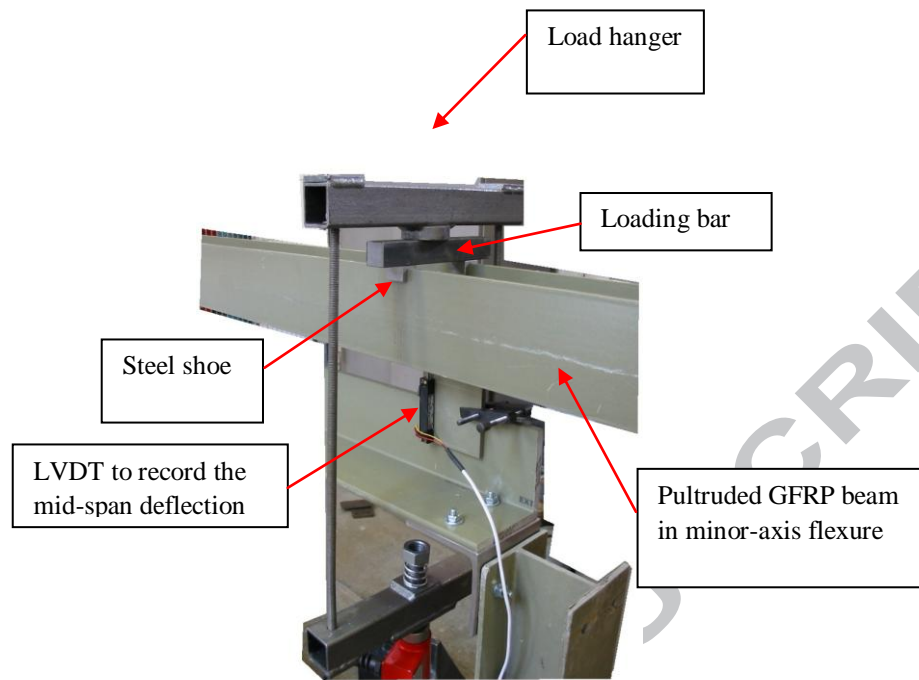


Figure 11(b)

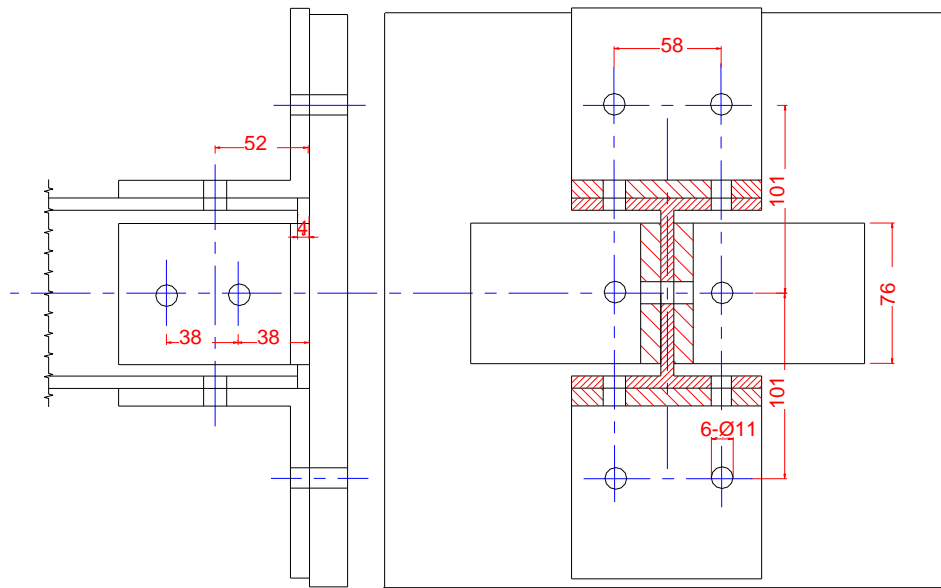


Figure 12

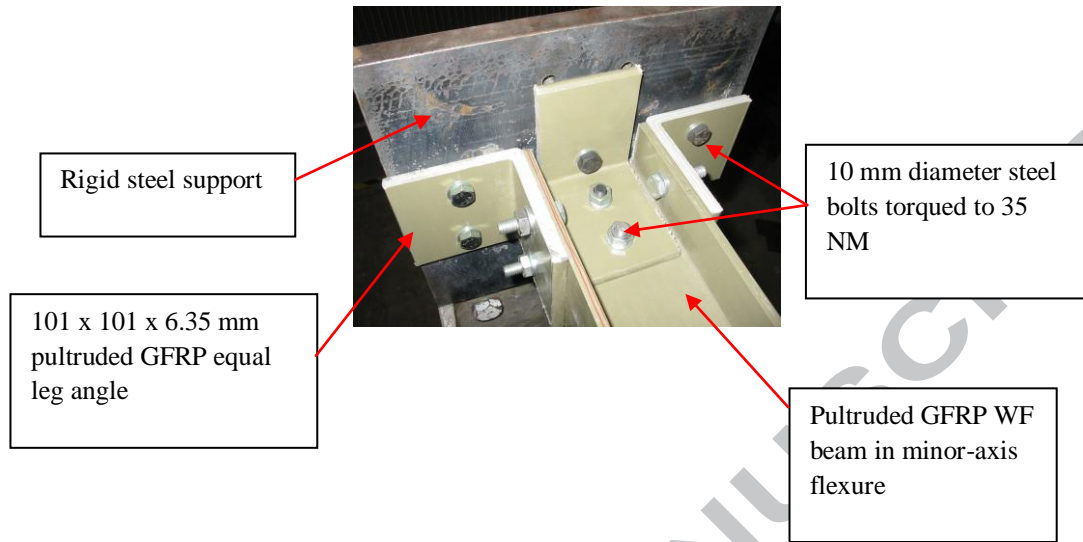


Figure 13

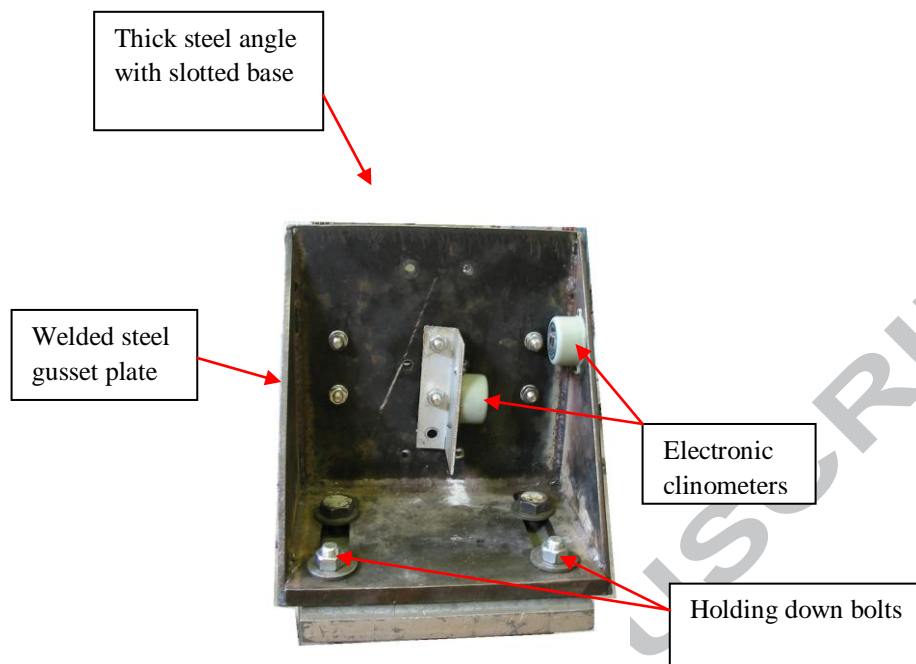


Figure 14: Welded mild steel gusseted angle used to provide a rigid support to which the pultruded GFRP angle cleats were bolted

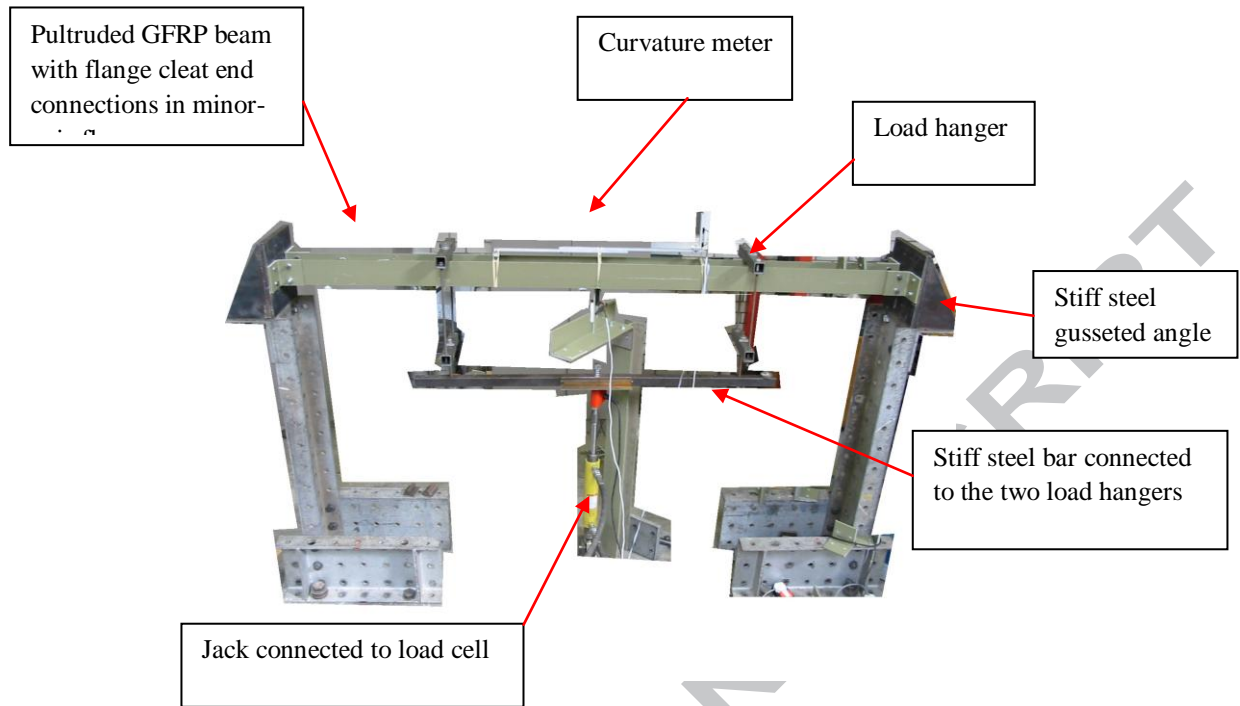


Figure 15: Overall view of a minor-axis four-point flexure test on a pultruded GFRP beam with semi-rigid end connections

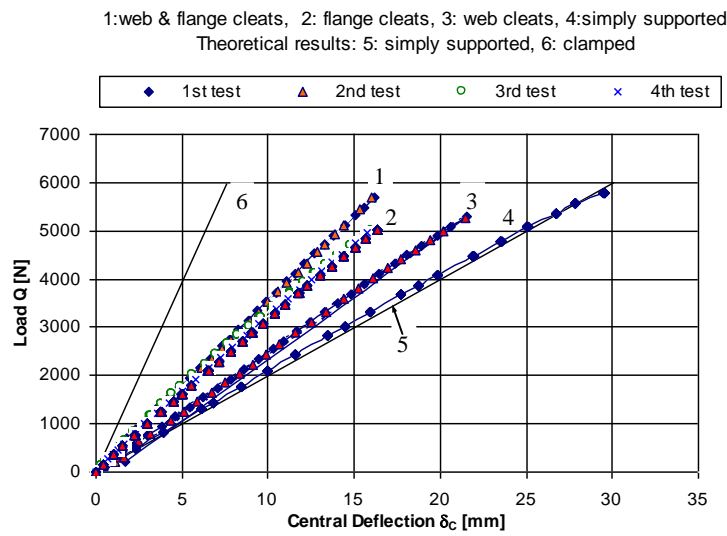


Figure 16 (a)

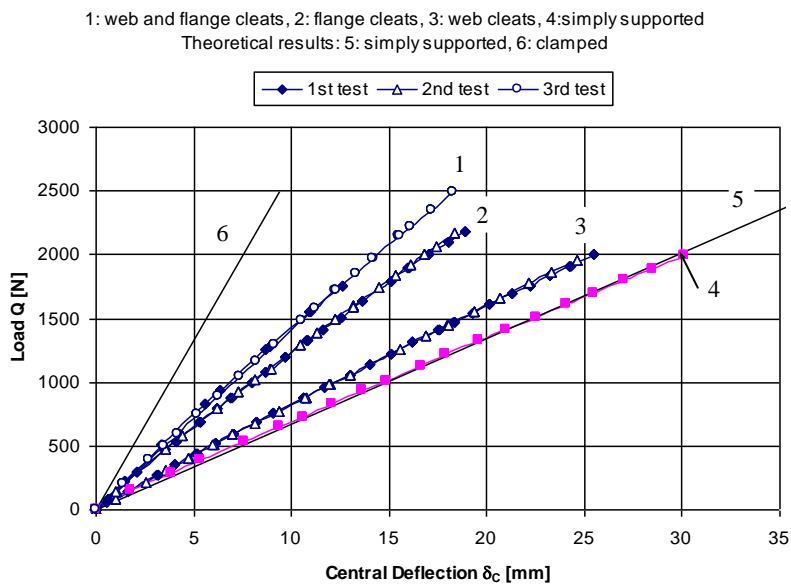


Figure 16 (b)

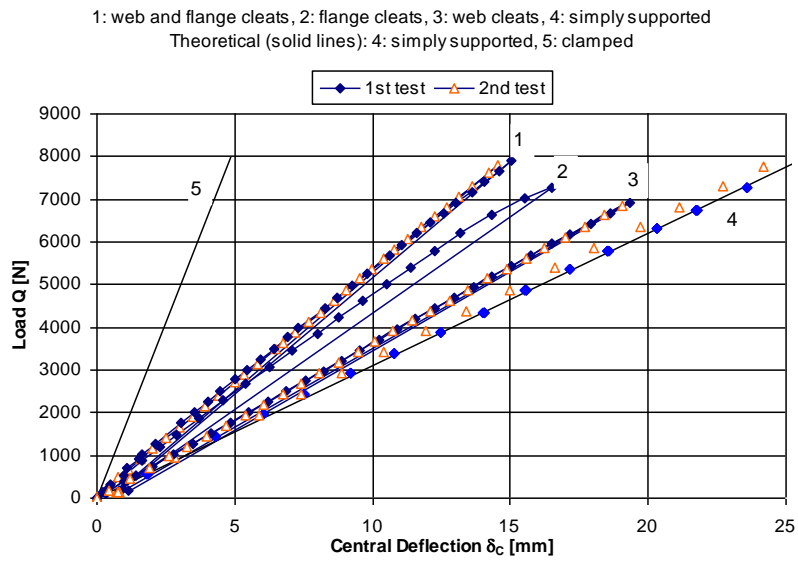


Figure 16 (c)

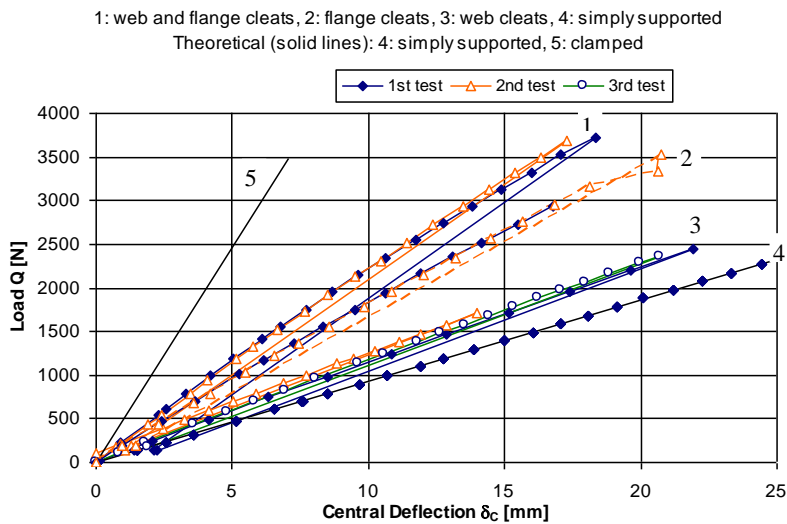


Figure 16 (d)

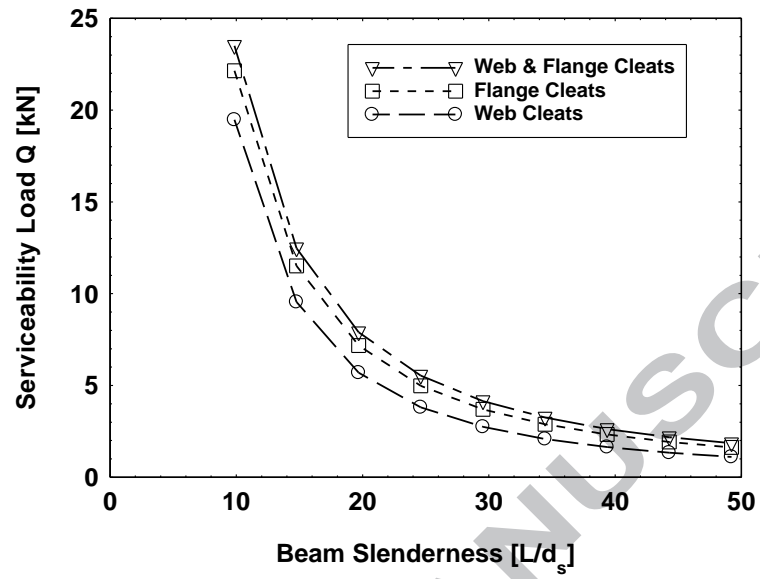


Figure 17

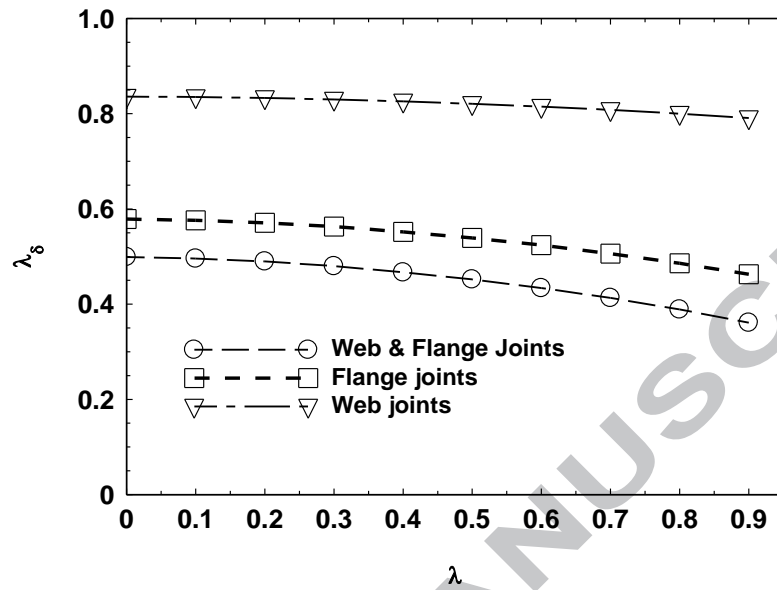


Figure 18 (b)

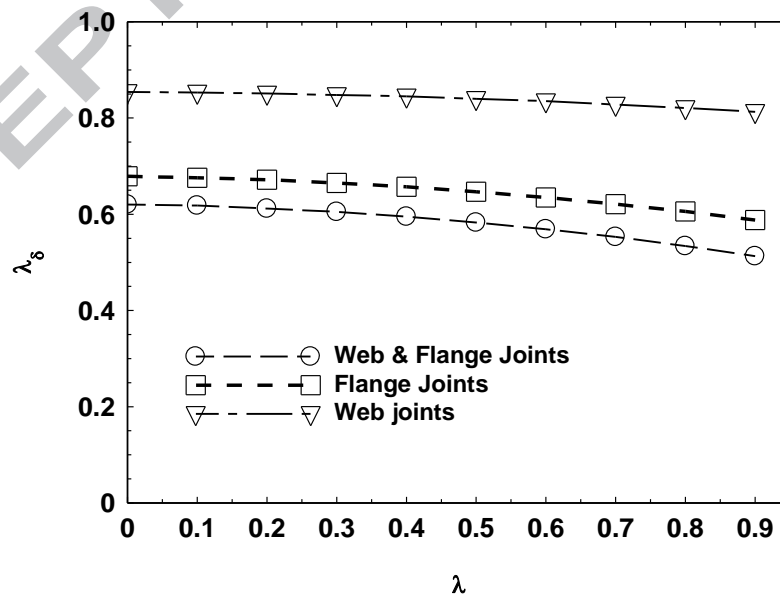


Figure 18 (a)

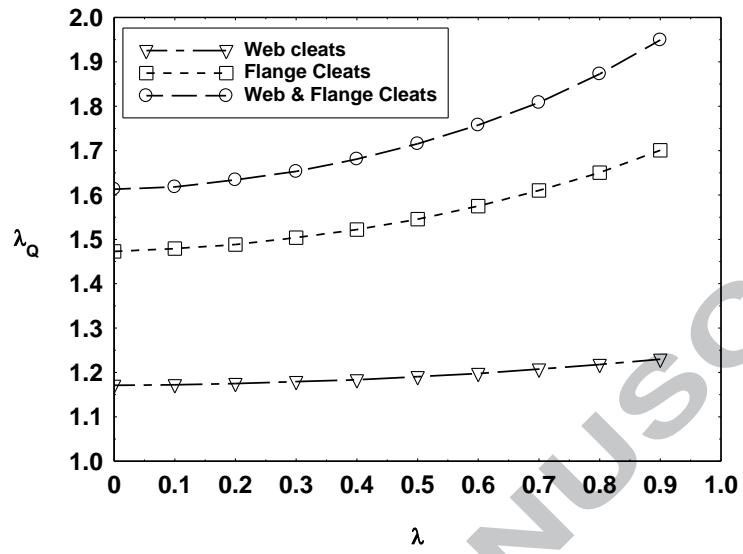


Figure 19

Table 1

Geometric properties of the 101.6 x 101.6 x 6.35 mm EXTREN[®] 500 Series pultruded GFRP WF profile

Major-axis second moment of area (I_x) [m ⁴ x 10 ⁻⁶]	Minor-axis second moment of area (I_y) [m ⁴ x 10 ⁻⁶]	Cross- sectional area (A) [m ² x 10 ⁻³]	Web cross- sectional area (A_w) [m ² x 10 ⁻⁴]	Flange cross- sectional area (A_f) [m ² x 10 ⁻³]	Major-axis radius of gyration (r_x) [m]	Minor-axis radius of gyration (r_y) [m]
3.30488	1.11134	1.86451	5.6774	1.297	0.0421	0.02441

Table 2

Longitudinal elastic moduli determined from deflection, curvature and strain data obtained from three- and four-point major- and minor-axis flexure tests on simply supported 101.6 x 101.6 x 6.35 mm pultruded GFRP WF beams

Type of Beam Flexure Test	Loading Axis	Test Span [m]	Elastic Modulus (Deflection δ_C) [GPa]	Elastic Modulus (Curvature Meter ρ_{xc}) [GPa]	Elastic Modulus (Strain Gauge ϵ_{xc}) [GPa]
Three-point	Major	2.52	20.07	-	-
	Minor		19.61	-	-
Four-point	Major	2.40 (1.00) [#]	-	-	22.80
			-	21.42	21.96
			-	22.27	22.17
	Minor		-	19.17	
	Major	2.00 (0.80)	-	-	22.24
			-	21.72	22.20
	Minor		-	19.78	19.48
	Major	1.60 (0.60)	-	21.61	21.65
	Minor		-	19.40	19.76
	Major-Axis Mean Values		-	21.8	22.2
	Minor-Axis Mean Values		-	19.5	19.6

[#] The span d of the curvature meter

Table 3

Estimates of the effects of shear deformation on the longitudinal elastic moduli determined from the three- and four-point flexure tests on simply supported 101.6 x 101.6 x 6.35 mm pultruded GFRP beams

Type of Flexure	Axis of Flexure	Test Span [m]	Span to Depth Ratio (L/d _s)	Shear Deformation Factors			
				$12\alpha_x$	$12\alpha_{wx}$	$12\alpha_y$	$12\alpha_{fy}$
Three-point	Major	2.52	24.80	0.02049	0.0673	-	-
	Minor					0.00689	0.00991
				$8.727\alpha_x$	$8.727\alpha_{wx}$	$8.727\alpha_y$	$8.727\alpha_{fy}$
Four-point	Major	2.40	23.62	0.01643	0.05396	-	-
	Minor			-	-	0.00553	0.00794
	Major	2.00	19.69	0.02366	0.07770	-	-
	Minor			-	-	0.00796	0.01144
	Major	1.60	15.75	0.03697	0.12141	-	-
	Minor			-	-	0.01243	0.01788

Table 4

Rotational stiffnesses obtained from the three- and four-point flexure tests on 2.52 m span 101.6 x 101.6 x 6.35 mm EXTREN[®] 500 Series pultruded GFRP WF beams with bolted GFRP end connections

Type of Flexure Test	Axis of Flexure	Longitudinal Elastic Modulus [GPa]	Test Number	Rotational Stiffness of Bolted End Connections [kNm/rad]		
				Web & Flange	Flange	Web
Three-point	Major	20.1	1	69.63	47.92	17.47
			2	72.21	47.75	17.81
			3	-	45.04	-
			4	-	45.68	-
	Minor	19.6	1	38.89	22.65	4.48
			2	33.06	23.80	4.95
			3	38.17	-	-
Four-point	Major	21.9	1	58.33	41.55*	12.33
			2	62.77	59.26**	12.63
	Minor	19.5	1	35.74	24.01*	4.66
			2	40.56	23.96*	6.01
			3	-	-	5.34
Mean major-axis rotational stiffnesses (all tests)				65.7	47.7	15.1
				(85)***		(14)***
Mean minor-axis rotational stiffnesses (all tests)				37.3	23.6	5.1

* Failure occurred in GFRP angle cleat

** GFRP angle cleats changed

*** Rotational stiffnesses reported in [15]